Experimental Study of the Functionality of a Semisubmersible Wind Turbine Combined with Flap-Type Wave Energy Converters

Constantine Michailides*, Zhen Gao and Torgeir Moan

Centre for Ships and Ocean Structures (CeSOS), Centre for Autonomous Marine Operations and Systems (AMOS), Department of Marine Technology,
Norwegian University of Science and Technology (NTNU)
Otto Nielsens vei 10, NO-7491, Trondheim, Norway
Email: constantine.michailides@ntnu.no; zhen.gao@ntnu.no; torgeir.moan@ntnu.no
**: Corresponding author, Tel. +4773595695, FAX. +4773595528*

Abstract

In the present paper the functionality of the Semisubmersible wind energy and Flap-type wave energy Converter (SFC) is examined experimentally. In order to study the functionality of the SFC, the focus is on operational environmental conditions. SFC is a combined concept that utilizes offshore wind energy and ocean wave energy for power production. Details are presented as far as the physical modelling of the wind turbine with the use of a redesigned small-scale rotor and of the Power Take-Off mechanism of the Wave Energy Converters (WECs) with the use of a configuration that is based on a mechanical rotary damper. Tests with quasi-static excitation, motion decay, regular and irregular waves without and with wind that is uniform are conducted on an 1:50 scale physical model. The experimental data are compared with numerical predictions obtained by a fully coupled numerical model using Simo/Riflex tool. A good agreement is observed between experimental and numerical predictions. The combined operation of WECs doesn't affect the tension of mooring lines nor the acceleration of nacelle and the bending moment in tower's base. The produced power of the WECs of the SFC and consequently the functionality of the SFC is estimated.

Keywords: Offshore combined concepts; Semisubmersible floating wind turbine; Flap-type wave energy converters; Power take-off physical modelling; Functionality.

Full explanation	Abbreviation
Centre of Gravity	COG
Ecole Centrale Nantes	ECN
Environmental Condition	EC
European Union	EU
Floating Wind Turbine	FWT
Mean Water Level	MWL
Mooring Line	ML
National Renewable Energy Laboratory	NREL
Oscillating Water Column	OWC
Power Take-Off	PTO
Response Amplitude Operator	RAO
Semisubmersible wind energy and Flap-type wave energy Converter	SFC
Spar Torus Combination	STC
Wave Energy Converter	WEC
Wave Gauge	WG

1. Introduction

The efficient harnessing and exploitation of the available enormous offshore (wind and wave) renewable energy resources can contribute significantly to the coverage of the increasing energy demands. Offshore renewable energy systems, namely Floating Wind Turbines (FWTs) and Wave Energy Converters (WECs), are expected to significantly contribute for the years to come to reach the energy security targets worldwide.

In recent years, offshore wind technology has been rapidly developed and commercially deployed in offshore wind farms with a trend towards larger scale wind turbines in larger water depths. For water depths larger than 100 m the use of FWTs is considered as the most appropriate from a cost-benefit point of view; FWT concepts for deep waters are still under development. Different floating support platform configurations are possible for use with FWTs [1]. One major type of support configuration is the semisubmersible platform consisting of columns that are connected with the use of braces [2,3]. Alternatively, the columns of the semisubmersible platform can be connected by pontoons with large dimensions and without braces [4,5,6]. In addition to offshore wind energy, ocean waves are an abundant and promising resource of alternative and clean energy; a large number of WECs has been proposed so far. The technology of WECs is currently under development but it is not mature yet for large scale commercial deployment. One major category of WECs is the rotating flap [7,8], usually this type of WECs is oscillating about a fixed axis close to the sea bottom. Hydrodynamic characteristics of such kind of devices are presented in [9] and [10]. [11] suggested the rotating flap to be fully submerged and to span vertically from the free surface about one third of the water depth. In general, WECs can efficiently deployed in multi-purpose offshore floating platforms [12,13].

In any case, the exploitation of the offshore wind and ocean wave energy resources should be realized in a sustainable manner, considering energy and cost efficiency. It might be beneficial to combine these energy systems of different technologies in one platform and investigate possible combined systems for simultaneous extraction of wind and wave energy. In order to evaluate the behaviour of the combined concepts, numerical models for the coupled dynamic analysis should be developed, while laboratory experiments in controlled environmental conditions for demonstrating the functionality of these concepts should be conducted.

Recently, EU research projects have been introduced to accelerate the development of combined offshore energy systems [14,15,16,17,18]. Several researchers [19,20,21] have studied combined concepts utilizing different floating support platforms and WEC types. In the EU project MARINA Platform three combined concepts have been selected and studied both numerically and experimentally under operational and survival conditions. The selection was based considering five simplified criteria, namely the cost of energy, constructability, installability, operation & maintenance and survivability. These combined concepts are the Semisubmersible wind energy and Flap-type wave energy Converter (SFC) [22] the Spar Torus Combination (STC) [23] and an array of Oscillating Water Columns (OWCs) in a V-shaped concrete large floating platform and one wind turbine combination [24].

The combined concept SFC consists of a braceless semisubmersible floating platform with four cylindrical shaped columns (one central column and three side columns) and three rectangular shaped pontoons with large dimensions that connect the side columns to the central column, a 5 MW wind turbine placed on the central column of the semisubmersible platform, three rotating flap-type WECs hinged at the pontoons of the semisubmersible through rigid structural arms and linear Power Take-Off (PTO) mechanisms, and three catenary mooring lines positioned at the three side columns of the semisubmersible. The upper point of the flap of WECs in its mean position is 2 m below the Mean Water Level (MWL) and the lower point of the flap is 15 m above the pontoon of the semisubmersible platform. In Figure 1 a sea view of SFC is presented.

[Figure 1]

Experimental investigation of the functionality of either FWTs or WECs has been conducted and reported so far by various researchers. As far as physical model testing of FWTs with different type of platform (spar, semisubmersible and tension leg), one particular uncertainty related to interpretation of the model test results is the scaling effect since it is not possible to scale simultaneously both the aerodynamic loads according to Reynold’s law and the hydrodynamic loads using Froude’s law [25]. Moreover there are different techniques for the rotor’s thrust force physical modelling. The rotor may be simplified as a disk providing a drag force [3] or as a controlled fan providing an active force [26,27]. A geometrically scaled rotor would produce less corresponding thrust force at model scale as compared to a full scale rotor [28] and a redesign of the blades is necessary in order to the correct scaled thrust curve to be achieved [29]. During most of the tests the blade pitch angle is fixed but it can be manually adjusted [30] utilizing an active pitch control mechanism of blades similar as what is expected for the full scale wind turbine.

As far as the experimental investigation of WECs, the set-up of the PTO configuration can be considered as the most critical part [31]. [32] studied two different PTO configurations of two different types of WECs, namely an OWC and two rigid modules that are rotating relative to each other. For the latter WEC [33] presented details about the physical modelling of the PTO configuration that consists of a metal bar with an elongate hole, a wire that is welded at the two ends of the hole and a small electric engine with a wheel. As far as testing of fixed bottom rotating flaps, [34] modelled the PTO configuration with an adjustable rotary viscous dashpot which is connected with a rotation shaft that is out of the water; this shaft is connected with a second shaft (that represents the axis of rotation of the WEC) through two thin pretensioned stainless steel wires. For the same type of WEC, [35] tested the PTO configuration with the use of a magneto-rheological damper for applying resistance on the model. Alternatively [36] modelled the PTO configuration of the rotating flap with a gear transmission system and a piston-type air compressor. For the case of a floating rotating flap [37] modelled the PTO configuration with the use of a load adaptable friction wagon mounted on a rail, a potentiometer for measuring the displacement of the flap and a force transducer for recording the transmitted force.

So far experimental investigations of combined wind/wave concepts have been reported by [38,39,40] based on different physical model set-up strategies of different parts of the combined concepts.

In the present paper the functionality of the offshore combined wind/wave energy concept SFC is experimentally examined and the measured data are compared with predictions obtained by a numerical analysis model. Operational environmental conditions in specific offshore sites are considered. The development of the physical model set-up is initially presented. The physical model of the SFC has been built in an 1:50 scale. The PTO configuration of each of the WECs is physically modelled with the use of a shaft, two pulleys, a timing belt, two tensioners and a linear mechanical rotary damper that provides a constant damping level. The wind turbine is physically modelled with a redesigned small-scale rotor that rotates during the experiments. The wind turbine has the correct mass property and produces the equivalent thrust force in model scale for selected few examined cases with different wind speed as compared to the NREL 5 MW reference wind turbine. Quasi-static, motion decay, regular and irregular waves without and with aligned wind excitation tests have been conducted. The experimental data are compared with numerical predictions obtained by a fully coupled multibody numerical analysis model in Simo/Riflex tool. The examined response data are the motions of the semisubmersible support platform, produced power by one flap-type WEC, tension of mooring lines, internal loads of the arms that connect the rotating flap with the pontoon of the semisubmersible platform, acceleration of the nacelle and bending moment in wind turbines tower base. A very good agreement between experimental and numerical results is observed for the motions of the semisubmersible platform and rotation of WECs. For the internal loads of WECs the agreement between experimental and numerical results can be considered acceptable. The operation of the WECs does not affect the tension of the mooring lines, the acceleration of nacelle and the bending moment in tower's base. The produced power of the WECs of the SFC and consequently the functionality of the SFC is estimated.

2. Physical model set-up

The tests have been performed in the Hydrodynamic and Ocean Engineering Tank in Ecole Centrale Nantes (ECN), France. The ocean basin is 50 m long (wave direction), 30 m wide and 5 m deep. The relevant wave and wind loading features could be represented in the ECN ocean basin with the use of wave and wind generation systems. The wave generation system consists of 48 independent flaps allowing the creation of regular as well as irregular directional waves up to 1 m height and wave period in the range 0.5~5 sec (in model scale). The wind generation system [41] is composed of eight centrifugal fans placed on the side of the ocean basin. The generated airflow is moved close to the physical model, which is placed in the centre of the basin, with the use of flexible air ducts. A rectangular shaped blow nozzle with dimensions 2.80 x 2.80 m is placed at the end of the air ducts in order to homogenize the outflow. The connection between the circular section of the air ducts to the rectangular section of the blow nozzle is achieved with the use of a diffusing adapting unit. Screens and honeycomb were used to improve the quality of the flow. Screens are tending to decrease the longitudinal component of the turbulence level and homogenize the mean velocity, while honeycomb is contributing for the decrease of the lateral component of the turbulence [42]. It must be noted that based on calibration of the wind generation system [41] the distribution of the mean wind speed over the testing area of the blowing nozzle can be considered as uniform. Also the turbulence intensity is lower than 3% in the same testing area. The wind generation system is capable for generating wind with a speed up to 10 m/sec in model scale. A sketch of the plan view of the basin as well as of the arrangement of the SFC during the tests is presented in Figure 2. In the same figure the two wave gauges, WG1 and WG2, that have been used for measuring the water free surface elevation are presented. The physical model of the SFC has been constructed in an 1:50 scale. The scale that was used for the physical modelling of the SFC was dominated by the existing physical model of the wind turbine in 1:50 scale. Froude laws of similitude have been used for the physical modelling of the properties of the semisubmersible platform and rotating flap-type WECs (Table

1). In Figure 3 the physical model of the SFC placed in the ECN's ocean basin is presented; in the same figure the blowing nozzle of the wind generation system can be seen. In Figure 4 the dimensions of different parts of the SFC are presented. It should be mentioned that the dimensions given in the text are presented in full scale. In Table 2 characteristics of the main components of the SFC are presented in full scale values.

[Figure 2]

[Figure 3]

[Figure 4]

[Table 1]

[Table 2]

As far as the semisubmersible platform, all the side walls of the pontoons of the platform have been built by wood while are internally filled with foam and steel bars for achieving the required moment of inertia. The upper part of the side columns of the platform has been built by synthetic glass while the lower part of the side columns close to the intersection with the pontoons has been built by 3D printed foam in order the PTO configuration of WECs to be fitted appropriately. The pontoons and columns of the semisubmersible platform have been built in order the platform to behave as a rigid body. A video motion capturing system (Qualisys motion capture system) with the use of four passive markers (Figure 3), which are placed at the top of the four columns of SFC, has been used for measuring the motions of the platform in six rigid body degrees of freedom. The sampling rate of all the sensors that were used during the experiments is equal to 120 Hz.

As far as the physical modelling of the WECs, each WEC consists of one fully submerged flap with elliptical shape with major axis equal to 7 m, minor axis equal to 3.5 m and length 20 m, two cylindrical shaped arms with an external diameter 0.7 m and one underwater shaft (axis of rotation). The major axis of the flap has direction that coincides with the direction of the vertical Z axis of the global coordinate system. The rotating flap has been built by synthetic foam, while the arms and the shaft have been built by titanium. Flap, arms and shaft behave as rigid bodies. The arms are rigidly connected at the higher end with the flap and at the lower end with the shaft. The shaft is founded to the pontoon of the platform in two low friction bearings. Moreover, the shaft through a low bearing is directed and inserted into the adjacent side column of the semisubmersible platform. The shaft into the side column is connected with the PTO configuration, which is used to physically model the linear PTO mechanism of the WEC. With regard to the PTO configuration, the shaft is connected with a lower pulley, which is connected through a timing belt with an upper pulley. The upper pulley is connected with a linear mechanical rotary damper. In order the timing belt to be in tension during the tests two tensioners are used (Figure 5). The level of the damping that the PTO configuration produces was calibrated in 'dry' conditions. The damping coefficient of the rotary damper, C_{PTO}, was manually adjusted prior to the execution of the tests. During the experiments the C_{PTO} has a constant value. It must be noted that the damping value that is used is not optimum and as a result the produced power by the WECs is not the potential maximum for different sea states. The instantaneous produced power by each WEC is calculated as below:

$$P(t) = C_{PTO}\dot{\theta}(t)^2 \qquad \text{(Eq. 1)}$$

where $\dot{\theta}(t)$ is the velocity of the rotation of the shaft. The rotation of the shaft is measured with the use of a rotary encoder sensor.

Moreover and in order to measure the internal loads in the arms of WECs strain gauges have been used. In both arms of WECs load sensors have been used for measuring the axial internal load, FZ, at the upper end of each arm close to the flaps. Moreover, strain gauges have been used for measuring the bending moment, MX, around x'x' axis of rotation of WECs at the lower end of the arm close to the shaft (Figure 5). It is noted that the torque that is applied at each shaft of PTO is equal to the summation of the MX_1 and MX_2 bending moments in the two arms of the same WEC. All the shafts of the three WECs are connected with three independent PTO configurations at their edges. The damping coefficient of the PTO is equal to 1,230 kNms/deg, 528 kNms/deg, 528 kNms/deg for WEC_1, WEC_2 and WEC_3, respectively. The rotation of the shaft is measured only for WEC_2, while the bending moment at the lower end of the arm and consequently the torque applied to the PTO configuration has been measured in all three WECs. In Figure 5 the physical model set-up of the WEC_2 is presented.

[Figure 5]

As far as the modelling of the wind turbine, a redesigned small-scale rotor has been used. The rotor has the correct mass property and produces the equivalent thrust force in model scale as compared to the NREL 5 MW reference wind turbine [43]. It must be noted that the correct thrust force can be produced only for few wind speed conditions and not for the whole range of wind speeds in which the turbine operates. Since the same Reynolds number cannot be achieved in the physical model, the blades of the wind turbine were redesigned for producing the correct thrust force relative to Froude laws of similitude. A 0.2 mm thick carbon fibre sheet has been used for the blades in order to achieve appropriate mass and length. In Table 3 the structural properties that were used for the blades are presented; in the same Table the target values based on NREL reference wind turbine are presented. The flapwise flexible mode was measured and the frequency was found to be significantly higher than the NREL reference frequency. In Table 4 the structural properties of nacelle and hub are presented. As far as the tower of the wind turbine, initially a study was performed in order to select the properties of the tower. The parameters constraining the selection of the properties of the tower are: (a) the first bending frequency of the tower has to be kept in the 'soft-stiff range' 1P and 3P and if possible more close to the 3P value, (b) the total tower mass has to be close to 1.81 kg and (c) the external radius of the tower should be as small as possible since higher wind speeds are used for the selected blade profiles and the wind load on the tower will be higher in the basin. As a result of this study the tower has been built with the use of a stainless steel cylinder with diameter 22 mm and thickness 2.3 mm (in scale model). Testing conditions with constant wind speed is the focus in the testing campaign of the SFC. The thrust force is obtained by changing the blade pitch angle and adjusting the wind speed. The optimal blade pitch angle in terms of the generated thrust force was obtained before the tests with appropriate calibration tests. The wind turbine was calibrated in a wind tunnel for determining the input wind speed that is required for obtaining the expected thrust for different blade pitch angles [41]. The calibration of the wind turbine has been carried out by researchers from ECN. Based on the results of the calibration, for the tests of the SFC the blade pitch angle was set equal to six degrees. During the tests the rotor thrust has been measured with the use of a force sensor placed at the tower top of the wind turbine. In order to measure the bending moment at the base of the tower of the wind turbine a load sensor has been placed at the lower part of the tower. More details with regard to the design of the wind turbine as well as to the generated thrust force as a function of the wind speed at model scale are presented in [41]. In Figure 6 the physical model set-up of the wind turbine of SFC and the wind generation system are presented.

[Table 3]

[Table 4]

[Figure 6]

With regard to the mooring lines of SFC, three catenary mooring lines made by inox chain were used with weight in air per unit length equal to 0.061 kg/m. For the design of the mooring lines of the physical model, the length and the mass of the chains have been adjusted in order to obtain the same offset-tension relationship compared to the full scale mooring lines. The horizontal stiffness of each mooring line is 563 N/m, while the vertical stiffness is 167 N/m. The tension of the mooring lines, ML_2 and ML_3, has been measured by a load cell at their fairlead.

As far as the environmental generated conditions, two wave gauges (WG1 and WG2) have been used for measuring the water free surface elevation and a wind load cell (sonic anemometer) has been used for measuring the wind speed. The wind thrust force has been measured with the use of a force sensor that measures the shear force response (positive X direction) on the tower top.

Different test conditions have been considered in order to study the functionality of SFC in operational conditions. Initially, quasi-static and decay tests have been performed in order to estimate basic properties of the physical model of SFC in calm water. Afterwards, regular wave tests have been performed for a range of wave periods for estimating the Response Amplitude Operators (RAOs) of different response quantities without and with aligned wind loads. Finally, irregular wave tests without and with aligned wind have been performed in order to investigate the SFC's functionality and response in operational conditions.

3. Test matrix

Different test conditions have been considered in order to study the functionality and response of SFC in operational conditions.

Quasi-static tests have been conducted for the estimation of the provided stiffness by the mooring lines. Moreover, hammer test has been performed for the calculation of the eigenfrequency of the first flexible mode of the tower. Decay tests have been performed for the estimation of the natural periods of three degrees of freedom of the semisubmersible platform and of the rotation of WEC_2. Based on the decay tests the estimation of the equivalent linearized damping ratio, ξ_{exp}, is determined.

Afterwards, regular wave tests have been performed for a range of wave frequencies for estimating the RAOs of different response quantities (e.g. motions, tension, internal loads, WEC_2 produced power). The regular wave tests have been performed without as well as with aligned wind loads. The waves propagate in the positive surge direction (+X). A total number of twelve different wave periods, T_i, i=1~12, are examined (Table 5), from 5.013 sec to 17.678 sec, while the examined wave height, H, is equal to 2 m (linear waves). The water depth is 250 m (5 m in scale model). During the regular wave tests with aligned wind loads the wind speed is equal to $U_{W,R}$=9.35 m/sec.

Finally, irregular wave tests without and with wind loads have been performed. In total six environmental conditions, ECi, i=1~6, are examined; the examined ECi, i=1~6, are presented in Table 6. In the same Table the turbulence intensity, TI, of the measured wind speed is also presented. For the first three ECi, i=1~3, wave with wind loading is applied while for the last three ECi, i=4~6, only wave loading exists.

[Table 5]

[Table 6]

4. Numerical model of the SFC

In the present paper a time domain model for the estimation of the response of SFC is developed and used. The results of the numerical model are compared with corresponding data measured during the experiments. The numerical model of the scaled model geometry of the SFC was developed using the software Simo/Riflex (developed by MARINTEK). This tool further extends the capabilities of the stand alone tools Simo [44] and Riflex [45]. Details as far as the developed numerical model of SFC can be found in [22,46]. Simo is used to model the time-domain hydrodynamic loads on rigid-body floating structures (platform and WECs), including the first-order and second-order wave loads. The equation of motion is solved in the time domain in Riflex, which is a nonlinear time domain program with a finite element formulation that can handle large displacements and rotations. Additionally, Riflex is used to model hydrodynamic loads on slender structures based on Morison equation. Moreover, Riflex has the capability to perform a coupled analysis, where one or more floating bodies are integrated with a dynamic model of a mooring system and arbitrary coupling forces in time domain.

The semisubmersible platform, three flaps of WECs, wind turbine hub and wind turbine nacelle are modelled through an integrated mass model and are considered as rigid bodies in the analysis. The arms of WECs, tower, shaft and blades are modelled by a distributed mass model and are considered as flexible bodies (beam elements). As far as the wind turbine modelling, the blades are connected with the hub. The hub and nacelle are connected with the top of the tower with the use of artificial rigid elements. A flex joint is applied to the hub to make it able to rotate about the longitudinal axis of the shaft. The loads on the blades and hub, and the resulted generator torque are transferred through the flex joint to the tower.

As far as the numerical modelling of the WECs, the flaps are rigidly connected with two arms at their two edges. At the lower ends the arms are hinged with the pontoons of the semisubmersible. The hinge joints, that are the connectors between the pontoon of the semisubmersible platform and the arm of the WECs, are modelled with the use of flex joints that behave as linear rotational dampers with respect to the axis of rotation of each WEC. The linear damping coefficient due to the PTO is considered as a constant value in the numerical analysis and similar to the one that was physically modelled in the experiments.

Wave loads on platform and flaps of WECs are estimated using panel method and based on potential theory. First-order for all rigid bodies and second-order for the platform only, based on Newman's approximation, wave forces are addressed and included into the analysis. After an appropriate convergence study with regard to the size of the panels of the wet surface of the platform and flaps, hydrodynamic analysis in [47] is performed for the calculation of hydrodynamic coefficients in frequency domain. These coefficients are the added mass, radiation damping, hydrostatic stiffness and excitation wave loads and are used as input for the numerical analysis in time domain. As far as the slender elements of the model (mooring lines and arms of WECs), the Morison equation is used for calculating their wave loads. It should be mentioned that the WEC upper part may move out of water obtaining non linear behaviour. The associated nonlinear hydrodynamic analysis due to the out of water WEC motion is not considered in the present numerical model. However, when solving the equation of motion in Riflex for the semisubmersible platform and WECs, the geometrical nonlinearity due to large translations and rotations between the different rigid bodies is considered. Regarding the hydrodynamic interaction between the different rigid bodies, in the current version of the Riflex (finite element solver) the cross terms (between the different rigid bodies) of the hydrodynamic coefficients of added mass and radiation damping are not taken into account. However, all the diagonal terms of added mass and radiation damping coefficients of each one rigid body are included. For the excitation forces the hydrodynamic interaction between the different rigid bodies is taken into account.

As far as the wind and wave excitation loads, the measured shear force response on the tower top and wave elevation of free surface in WG1 time series are given as input data as dynamic loads in the numerical model. Ideally, the measured wind speed can be used by a stochastic, full-field, turbulent-wind simulator and afterwards the produced wind loads could be applied to the numerical model.

Numerical analysis is dealt within Riflex and the equation of motion is solved in the time domain based on the following Equation:

$$\mathbf{R}^{I}(\mathbf{r},\ddot{\mathbf{r}},t)+\mathbf{R}^{D}(\mathbf{r},\dot{\mathbf{r}},t)+\mathbf{R}^{S}(\mathbf{r},t)=\mathbf{R}^{E}(\mathbf{r},\dot{\mathbf{r}},t) \qquad \text{(Eq. 2)}$$

where $\mathbf{R}^I$ is the inertia force vector, $\mathbf{R}^D$ is the damping force vector, $\mathbf{R}^S$ is the internal structural reaction force vector, $\mathbf{R}^E$ is the external force vector and $\mathbf{r}, \dot{\mathbf{r}}, \ddot{\mathbf{r}}$ are the structural displacement, velocity and accelerations vectors. It is noted that all the force vectors are established by assembly of the element distributions and the specified discrete nodal forces. Equation 2 expresses a nonlinear system of differential equations due to displacement dependencies in the inertia and the damping forces between the external load vector and the structural displacement and velocity.

5. Calibration quasi-static and decay tests

Prior to the calibration tests, the draft of the platform has been measured and verified in calm water; the platform has draft equal to 30 m while the upper part of the flaps in rest is 2 m below the MWL. It should be mentioned, that all the presented values given in the text are presented in full scale. Both the measured data and the numerical predictions have been up scaled to full scale.

Quasi-static tests have been conducted in order to identify the stiffness of the mooring lines ML_2 and ML_3. Different forced offsets have been applied to the platform in the surge positive and negative directions and the fairlead tension of the mooring lines has been measured. In Figure 7 the relationship between the offset in surge direction and the tension of ML_2 and ML_3 is presented. The prediction of the numerical analysis model of the tension of the two mooring lines, ML_2 and ML_3, is the same due to the symmetry of the structure and the direction of the offset. The mooring lines start to behave in a non-linear fashion for offset larger than 30 m approximately. For positive offsets the tension of the ML_2 as measured experimentally is slightly larger (e.g. 2%) compared to the tension of ML_3. The pretension of the mooring lines at the fairlead is equal to 1,779 kN, while the pretension of the mooring lines predicted by the numerical analysis is 1,862 kN. The equivalent horizontal stiffness of each mooring line ML_2 and ML_3 is 563 N/m, while the equivalent vertical stiffness is 167 N/m. The physical model data agree well with the numerical predictions.

[Figure 7]

Experimental decay tests have been carried out for determining the natural periods of three degrees of freedom of the platform, namely surge, heave and pitch as well as of the rotation of the WEC_2. In a similar manner, decay tests have been performed in the numerical model in order to compare with the results that are measured by experimental decay tests. In Table 7 the measured and calculated natural periods of the aforementioned degrees of freedom are presented. T_{exp} is the measured natural period of the physical model, while T_{num} is the corresponding calculated natural period with the use of the numerical model. Also in Table 7 the equivalent linearized damping ratio, ξ_{exp}, as calculated by the experimental decay tests is presented. As shown in Table 7 there is a very good agreement between the natural periods as measured experimentally and predicted numerically. The natural periods of the motions of the platform are out of the examined wave period zone. It should be noted that during the execution of the decay tests the wind turbine is parked while the PTOs of all WECs are placed into the side columns of SFC and are in operation. Moreover, no wind and wave loads exist.

Finally, hammer test has been performed for the estimation of the first bending eigenfrequency of the tower of the wind turbine. Based on the data from the hammer test, the eigenfrequency has been found to be equal to 3.8 rad/sec (full scale value).

[Table 7]

6. Regular wave tests without and with wind loading

In the present section the experimental and numerical RAOs of responses of different parts of SFC are presented. The tests have been performed in regular waves without and with wind loading. During the tests the rotor of the wind turbine and the PTOs of all WECs (linear damper) are in operation (Table 4).

In Figure 8 the RAOs of surge, heave and pitch motions of the semisubmersible platform are presented. For surge and heave motion exist an increase of the RAOs with the increase of the examined period. For surge motion the differences between numerical and experimental RAOs are larger for periods close to the resonance of the rotation of WECs. For both experimental data and numerical predictions the effect of the wind loading on the amplitude of surge RAO is insignificant. Meanwhile, for the case of regular waves with wind loading the mean value of the surge motion is larger 1.8 m compared to the mean value that the surge has for regular wave loading only. The amplitude of heave RAO as well as the mean value of the heave motion is not affected by the wind loading. For the pitch RAO, a first peak of the curve is presented for T_8=12.806 sec, attributed to the peak of the first-order hydrodynamic wave loads of the platform for the same period. For larger wave periods, T_i>12.806 sec, a decrease of the pitch RAO exists. The mean value of the amplitude of the pitch motion for the case of regular waves with wind loading is larger 2.2 deg compared to the mean value of the pitch amplitude for regular wave loading only. As it was presented in Table 7, all the natural periods of the motions of the semisubmersible platform are not excited. For the motions of the semisubmersible platform the effect of the wind loading and the effect of the aerodynamic damping are small attributed to the dominance of the inertial forces and potential damping. It should be noted that for sway, roll and yaw motions of the platform very small RAOs are measured experimentally for a few number of examined periods; attributed to the uncertainties that exist during the tests (e.g. sensor weights, cables). With regard to the rotation, θ, of the WEC_2 the peak of the motion is observed for its natural period (Table 7). The wind loading results to the increase of the WEC_2 rotation compared to the case that only wave loading exists; this is attributed to the larger mean pitch value of the platform that has as a result the WEC_2 and WEC_3 to be placed in higher positions in the vertical direction and closer to the MWL. Differences between experimental and numerical results become larger in the period range close to the resonance of the rotation of WEC_2, this is attributed to the uncertainties of the viscous damping model that was used in the numerical analysis as well as to the friction losses of parts of the physical model (e.g. bearings, PTO configuration) that cannot be modeled in the numerical analysis. In general, for all the motions of the semisubmersible platform and of the rotation of WEC_2 there is a good agreement between the experimental and numerical results.

[Figure 8]

With regard to the tension of the mooring line ML_2, in Figure 9 a comparison between experimental and numerical RAOs of the ML_2 tension is presented. For both loading conditions a good agreement is observed. The tension of the ML_2 for the case of wave and wind loading is always larger compared to the case of wave loading only. This is attributed to the larger mean values of surge and pitch motions of the semisubmersible platform that result into a stiffer system. For wave loading only condition and moving from 5.013 sec to 7.934 sec an increase of the tension is observed attributed to the increase of the pitch and surge motion of the semisubmersible platform. For larger examined periods there is a decrease of the measured tension RAO. For wave and wind loading conditions the increase of the tension RAO moving from 5.013 sec to 7.934 sec as well as the decrease of the RAO for larger examined periods is smoother.

With regard to the wind turbine, the RAOs of the acceleration of the nacelle in X direction (Fig. 10a) and bending moment, MX, of tower's base (Fig. 10b) are presented in Figure 10. Both curves have the same pattern; initially an increase up to T_2 exists, then a gradually decrease up to T_7 and finally for larger examined periods an insignificant increase. The behaviour of the acceleration of nacelle and of MX is mainly affected by the motions of the platform (surge and pitch) and is not affected by the resonance of the rotation of WECs. The acceleration of the nacelle was not measured for the case of regular wave tests with wind loading due to technical problems during the tests.

[Figure 9]

[Figure 10]

With regard to the behaviour of WECs, in Figure 11 experimental and numerical RAOs of FZ_1 of WEC_2 (Fig. 11a), produced power of WEC_2 (Fig. 11b), PTO's torque of WEC_2 (Fig. 11c) and PTO's torque of WEC_3 (Fig. 11d) are presented. As far as FZ_1 of WEC_2, the increase of the wave period has as a result the gradually decrease of FZ_1. The effect of the wind loading on the FZ_1 RAO values is insignificant. The peak of the produced power of WEC_2 is observed for wave period T=15.786 sec close to WEC_2's measured natural period of θ. The produced power RAO that corresponds to wave loading only is smaller compared to the produced power RAO for the case of wave with wind loading; this is attributed to the larger mean value of the pitch motion of the platform that has as a result the two WECs, WEC_2 and WEC_3, to be placed in higher positions and closer to the MWL. The differences between experimental and numerical results become larger close to the resonance of the rotation of WEC_2 attributed to the uncertainties of the damping model that was used in the numerical analysis for the rotation motion of WECs. As far as the torque of WEC_2, an increase of the torque is observed up to the examined wave period T_7. The torque is affected by the wind loading; larger values are observed for the examined cases where wave and wind loading are considered and compared with wave loading only conditions. The numerical model overpredicts the measured torque. The produced power by WEC_3 is expected to reach values that are similar with the values of produced power by WEC_2 as presented in Figure 11b attributed to the similar values of torque between WEC_2 and WEC_3. The torque of WEC_2 and WEC_3 as calculated by the numerical model obtains equal values. It should be noted that the produced power by WECs is not optimum; the present paper is not dealing with the maximization of the produced power but with the proof of the combined concept SFC.

[Figure 11]

7. Irregular wave tests without and with wind loading

Irregular wave tests without and with wind loading have been conducted. Six environmental conditions are examined (Table 6). In Figure 12 time series of wave elevation of WG1 (Fig. 12a) for EC2, spectra of wave elevation of WG1 (Fig 12b) for EC1, EC2 and EC3, wind speed (Fig. 12c) for EC2 and shear force response on the tower top (Fig. 12d) for EC2 are presented. It must be noted that for the examined conditions the mean wind speed is 9.35 m/sec, the turbulence intensity 0.009 and the mean shear force response on the tower top is 648 kN (full scale). The target thrust value based on NREL reference wind turbine is 620 kN. The shear force response on the tower top has been given as input in the numerical analysis. The spectra of wave elevation of EC4, EC5 and EC6 (only wave excitation loading) are similar to the spectra of wave elevation of EC1, EC2 and EC3, respectively.

[Figure 12]

In Figure 13 the one hour statistical maximum and standard deviation, std, values of experimental data and numerical predictions for surge, heave and pitch of semisubmersible platform are presented for ECi, i=1~6. The largest relative difference of the std value between experimental and numerical predictions is 8% for surge, 11% for heave and 10% for pitch. The increase of the examined wave period has as a result the decrease of the std value for surge and the increase of the std value for heave. With regard to the maximum values, the largest relative difference of the maximum value is 6% for surge, 8% for heave and 9% for pitch. Similar to the case of regular waves, the mean value of the surge and pitch motions for EC1, EC2 and EC3 is 1.8 m and 2.1 deg larger compared to EC4, EC5 and EC6, respectively. The largest pitch angle of the platform for the examined operational conditions was found equal to 3.01 deg for EC2.

[Figure 13]

[Figure 14]

As far as mooring line ML_2 and wind turbine, in Figure 14 the maximum and std values of X acceleration of nacelle, MX bending moment of tower's base and fairlead tension of ML_2 for ECi, i=1~6, are presented. The largest relative difference of the std value between experimental and numerical predictions is 10% for X acceleration of nacelle, 9% for MX bending moment and 10% for tension of ML_2. The increase of the examined wave period has as a result the decrease of the std and maximum values for both X acceleration and MX bending moment. For MX the numerical model underestimates the maximum value while for ML_2 the numerical model overpredicts the maximum value. The largest measured X acceleration of the nacelle is equal to 0.032 m/sec^2 for EC4. The wind loading clearly affects the MX bending moment of the tower; compared to wave loading only an increase of the MX value with an average value 79% is observed for wave and wind loading.

With regard to the flap-type WECs, in Figure 15 the maximum and std values of FZ_1, MX_1 of WEC_2, torque of WEC_2 and torque of WEC_3 are presented for ECi, i=1~6. The largest relative difference of the std value is 11% for FZ_1, 15% for MX_1, 13% for torque of WEC_2 and 15% for torque of WEC_3. The numerical model overpredicts the maximum values of the torque of both WECs. The wind loading affects the measured torque; an increase of the std of the torque with an average value equal to 9% is observed. The measured torque of the two WECs, WEC_2 and WEC_3, obtains equal value for all the examined ECi, i=1~6.

[Figure 15]

In Figure 16 spectra comparison are presented of experimental and numerical predictions for EC2 and EC5 of surge (Fig. 16a) and pitch (Fig. 16b) of semisubmersible platform, tension of mooring line ML_2 (Fig. 16c), bending moment in tower's base (Fig. 16d), FZ_1 internal load (Fig. 16e) and torque (Fig. 16f) of WEC_2. As far as the motions of the platform, the resonance of each motion spectrum is presented for the frequency that corresponds to the natural frequency as calculated by the decay tests; the second peak in the motion curve corresponds to the frequency of wave excitation. The effect of the wind loading is clearly presented for pitch motion while is smaller for surge motion. As far as the mooring line ML_2, the resonance of tension spectrum is presented for the frequency value where the RAO of ML_2 tension has also resonance (Figure 9). The resonance of the bending moment in tower's base, MX, is presented for the frequency (ω=3.8 rad/sec) that corresponds to the first bending eigenfrequency of the tower of the wind turbine; this resonance is presented only for the case of wave with wind loading EC2 and not for EC5. A second peak with smaller value is presented for the frequency where the RAO of MX has also peak (Figure 10b). Regarding the WEC_2, for both FZ_1 and torque the resonance is observed close to the frequency of wave excitation; also, the numerical model overpredicts the FZ_1 and torque. The effect of the wind loading is clearly presented for the torque of WEC_2 and is insignificant for FZ_1 internal load.

[Figure 16]

With regard to the functionality of the WECs of SFC, in Table 8 statistical quantities of the time series of the produced power of WEC_2 are presented. An increase of the produced power is presented moving from EC1 to EC3 as well as moving from EC4 to EC6. The largest measured mean produced power is 70.2 kW while the largest mean produced power predicted numerically is 77.6 kW both for EC3. The numerical model overpredicts the produced power on average by 13%, primarily believed to be attributed to the friction losses of parts of the physical model set-up (e.g. bearings, PTO configuration) that cannot be modeled in the numerical analysis. The standard deviation is on average 1.47 times larger than the mean value of the produced power. The maximum value of the produced power is 14.8 ~ 18.2 times larger compared to the mean value and on average 16.4 times larger. It is expected that the produced power of WEC_3 will obtain similar value as the presented produced power of WEC_2 in Table 8 since the torque in the two WECs is similar. It should be noted that the produced power by WECs is not optimum; the present paper is not dealing with the maximization of the produced power but with the proof of the SFC concept. It must be noted that combining the flap-type WECs with the FWT was found to have insignificant effect on the wind power production but increases the total power production by 3~5% [22]. However, based on a preliminary evaluation in the MARINA project [48], the cost of energy for the SFC is higher than that of a pure semisubmersible wind turbine.

[Table 8]

8. Conclusions

This paper deals with the study of the behaviour and the functionality of the combined offshore wind/wave energy concept SFC in operational environmental conditions based on physical model tests and numerical analysis. The SFC consists of a braceless semisubmersible floating wind turbine and three fully submerged rotating flap-type WECs. The development of the physical model set-up in an 1:50 scale and the test program are presented. The PTO configuration of each of the WECs is physically modelled with the use of a shaft, two pulleys, a timing belt, two tensioners and a linear mechanical rotary damper with constant damping level during the execution of the tests. The wind turbine is physically modelled with a redesigned small-scale rotor that rotates during the experiments.

The draft of the semisubmersible platform, the stiffness of the mooring lines, the natural frequency of motions of both semisubmersible platform and flap-type WECs, and the eigenfrequency of the first bending mode of the tower of the wind turbine are measured and calculated with appropriate calibration tests into basin. These properties are validated with the numerical model. The mooring lines start to exhibit a non linear behaviour for offset larger than 30 m. The natural periods of the motions of the semisubmersible platform are well set out of the examined wave period zone. The differences between experimental and numerical predictions for the calibration tests are small.

Regular wave tests without as well as with the existence of aligned wind loads have been performed for twelve wave periods for estimating the RAOs of different response quantities. For all the examined motions of the semisubmersible platform there is a good agreement between the experimental and numerical results. For regular wave tests and compared to the wave only loading condition, the mean amplitude of time series of surge and pitch motions of the platform is larger for the case of wave with wind loading attributed to the steady wind load. The RAO of the tension of the ML_2 for the case of wave and wind loading is always larger compared to the case of only wave loading. The RAOs of the acceleration of nacelle and the bending moment in tower's base are dominated by the surge and pitch motions of the platform and are not affected by the rotation of WECs. The RAO curve of the acceleration of nacelle has the same pattern with the RAO curve of the bending moment in tower's base. The WEC_2's produced power RAO that corresponds to wave loading only is slightly smaller compared to the WEC_2's produced power RAO for the case of wave with wind loading. The numerical model overpredicts the produced power by WECs.

Irregular wave without and with wind loading tests have been performed for six environmental conditions. Comparisons of statistical maximum and standard deviation values between experimental and numerical data are presented for different responses. Compared to wave and wind loading, better agreement between experimental and numerical predictions is obtained for the case of wave loading only. For irregular wave tests and compared to the wave only loading cases, the mean value of the produced power of WECs is larger for irregular waves with wind loading. The combined operation of the WECs does not affect the tension of the mooring lines, the acceleration of the nacelle and the bending moment in tower's base. The functionality of the SFC concept in operational environmental conditions with focus to the produced power by the flap-type WECs has been demonstrated and presented.

The presented results in this paper with regard to the produced power give an indication about the relative contribution of the power from flap-type WECs for selected wind and wave environmental conditions. It would be of interest to perform a long-term numerical analysis in order to compare the annual average produced power of the combined concept SFC with the corresponding annual average produced power of the pure semisubmersible wind turbine for selected sites as well as to compare the cost of energy based on an appropriate cost study. In this connection a more detailed engineering design of the hull structure is required. The presented data can be used for validation of numerical models of combined multibody offshore energy systems by other researchers. Finally, it would be interesting to numerically investigate the optimization of the power performance of SFC towards minimization of cost of energy (power).

Acknowledgements

The authors would like to acknowledge the financial support from the MARINA Platform project (Marine Renewable Integrated Application Platform, Grant Agreement no. 241402) under the European Community FP7 Energy Programme. The financial support for the construction of the physical model of the SFC concept from the MARINA Platform is greatly acknowledged. The contribution of Thomas Soulard and Sylvain Bourdier at ECN to the planning, construction and execution of the model tests is highly appreciated. The financial support from the Research Council of Norway through the Centre for Ships and Ocean Structures and the Centre for Autonomous Marine Operations and Systems, the Norwegian University of Science and Technology, is also acknowledged.

References

[1] Jonkman JM, Matha D. Dynamics of offshore floating wind turbines-analysis of three concepts. Wind Energy 2011;14(4):557–569.

[2] Robertson A, Jonkman J, Masciola M, Song H, Goupee A, Coulling A, Luan C. Definition of the Semisubmersible Floating System for Phase II of OC4. NREL/TP-5000-60601, National Renewable Energy Laboratory, Golden, CO, U.S.A, 2014.

[3] Roddier D, Cermelli C, Aubault A, Weinstein A. WindFloat: A floating foundation for offshore wind turbines. Journal of Renewable and Sustainable Energy 2010;2(3): 033104-1-033104-34.

[4] Olav Olsen AS (Online). Available at: http://www.olavolsen.no/node/82 [Accessed 10 November 2015].

[5] Luan C, Gao Z, Moan T. Conceptual designs of a 5-MW and a 10-MW semi-submersible wind turbine with emphasis on the design procedure. (Under review).

[6] Karimirad M, Michailides C. V-shaped semisubmersible offshore wind turbine: An alternative concept for offshore wind technology. Renewable Energy 2015;83:126-143.

[7] Falnes J. A review of wave-energy extraction. Marine Structures 2007;20:185–201.

[8] Falcão A. Wave energy utilization: A review of the technologies. Ren and Sust Energy Reviews 2010;14:899–918.

[9] Caska AJ, Finnigan TD. Hydrodynamic characteristics of a cylindrical bottom-pivoted wave energy absorber. Ocean Engineering 2008;35:6–16.

[10] Renzi E, Dias F. Relations for a periodic array of flap-type wave energy converters. Applied Ocean Research 2012;39:31–39.

[11] Kurniawan A, Moan T. Characteristics of a pitching wave absorber with rotatable flap. Energy Procedia 2012;20:134–147.

[12] Michailides C and Angelides DC. Modeling of energy extraction and behaviour of a Flexible Floating Breakwater. Applied Ocean Research 2012;35:77-94.

[13] Michailides C and Angelides DC. Optimization of a flexible floating structure for wave energy production and protection effectiveness. Engineering Structures 2015;85:249-263.

[14] MARINA PLATFORM (Online). Available at: http://www.marina-platform.info/index.aspx [Accessed in October 2015].

[15] ORECCA (Online). Available at: http://www.orecca.eu/ [Accessed in October 2015].

[16] TROPOS (Online). Available at: http://www.troposplatform.eu/ [Accessed in October 2015].

[17] H2Ocean (online). Available at: http://www.h2ocean-project.eu/ [Accessed in October 2015].

[18] MERMAID (Online). Available at: http://www.mermaidproject.eu/ [Accessed in October 2015].

[19] Soulard T, Babarit A, Borgarino B, Wyns M, Harismendy M. C-HYP: A combined wave and wind energy platform with balanced contributions. Proc of the 32nd International Conference on Ocean, Offshore and Arctic Engineering, no. OMAE2013-10778, Nantes, France.

[20] Aubult A, Alves M, Sarmento A, Roddier D, Peiffer A. Modeling of an oscillating water column on the floating foundation WindFloat. Proc. of the 30th International Conference on Ocean, Offshore and Arctic Engineering, no. OMAE2011-49014, Rotterdam, Netherland.

[21] Peiffer A, Roddier D, Aubult A. Design of a point absorber inside the WindFloat structure. Proc. of the 30th International Conference on Ocean, Offshore and Arctic Engineering, no. OMAE2011-49015, Rotterdam, Netherland.

[22] Michailides C, Luan C, Gao Z, Moan T. Effect of Flap Type Wave Energy Converters on the Response of a Semi-submersible Wind Turbine in Operational Conditions. Proc of the 33rd International Conference

on Ocean, Offshore and Arctic Engineering. Paper No. OMAE2014-24065, pp V09BT09A014, doi:10.1115/OMAE2014-24065.

[23] Muliawan MJ, Karimirad M, Moan T. Dynamic response and power performance of a combined spar-type floating wind turbine and coaxial floating wave energy converter. Renewable Energy 2013;50:47–57.

[24] O'Sullivan K, Murphy J. Techno-Economic Optimisation of an Oscillating Water Column Array Wave Energy Converter. Proc. of the 10th European Wave and Tidal Energy Conference, Aalborg, Denmark.

[25] Müller K, Sandner F, Bredmose H, Azcona J, Manjock A, Pereira R. Improve Tank Test Procedures for Scaled Floating Offshore Wind Turbines. The International Wind Engineering Conference – Support Structures & Electrical Systems. September 3-4, Hannover, Germany 2014.

[26] Azcona J, Bouchotrouch F, González M, Garciandía J, Munduate X, Kelberlau F, Nygaard TA. Aerodynamic Thrust Modelling in Wave Tank Tests of Offshore Floating Wind Turbines Using a Ducted Fan. Journal of Physics: Conference Series 2014;524:012089.

[27] Huijs F, Ridder EJ, Savenije F. Comparison of model tests and coupled simulations for a semi-submersible floating wind turbine. Proc of the 33rd Int Conf on Oc, Off and Arc Eng. Paper No. OMAE2014-23217, San Francisco, USA.

[28] Fowler MJ, Kimball RW, Thomas DA, Goupee AJ. Design and Testing of Scale Model Wind Turbines for Use in Wind/Wave Basin Model Tests of Floating Offshore Wind Turbines. Proceedings of the ASME 2013 32nd International Conference on Ocean, Offshore and Arctic Engineering. Paper No. OMAE2013-10122, June 9-14, Nantes, France.

[29] Martin HR, Kimball RW, Viselli AM, Goupee AJ. Methodology for Wind/Wave Basin Testing of Floating Offshore Wind Turbines. Proceedings of the ASME 2012 31st International Conference on Ocean, Offshore and Arctic Engineering. Paper No. OMAE2012-83627, July 1-6, Rio de Janeiro, Brazil.

[30] Goupee AJ, Fowler MJ, Kimball RW, Helder J, De Ridder EJ. Additional Wind/Wave Basin Testing of the DeepCwind Semi-submersible with a Performance-Matched Wind Turbine. Proceedings of the ASME 2014 33rd International Conference on Ocean, Offshore and Arctic Engineering. Paper No. OMAE2014-24172, June 8-13, San Francisco, California, USA.

[31] Sheng W, Alcorn R, Lewis T. Physical modeling of wave energy converters. Ocean Engineering 2014;84:29-36.

[32] Martinelli L, Zanuttigh B, Kofoed JP. Selection of design power of wave energy converters based on wave basin experiments. Renewable Energy 2011;36:3124-3132.

[33] Zanuttigh B, Angelelli E. Experimental investigation of floating wave energy converters for coastal protection purpose. Coastal Engineering 2013;80:148-159.

[34] Flocard F, Finnigan TD. Laboratory experiments on the power capture of pitching vertical cylinders in waves. Ocean Engineering 2010;37:989-997.

[35] Qiu S, Ye J, Wang D, Liang F. Experimental study on a pendulum wave energy converter. China Ocean Engineering 2013;27(3):359-368.

[36] Ogai S, Umeda S, Ishida H. An experimental study of compressed air generation using a pendulum wave energy converter. Journal of Hydrodynamics 2010;22(5):290-295.

[37] Pecher A, Kofoed JP, Espedal J, Hagberg S. Results of an experimental study of the langlee wave energy converter. 20th International Offshore and Polar Engineering Conference, ISOPE-2010; Beijing; China.

[38] Gao Z, Moan T, Wan L, Michailides C. Comparative numerical and experimental study of two combined wind and wave energy concepts. Journal of Ocean Engineering and Science 2015 (Accepted for publication, doi:10.1016/j.joes.2015.12.006).

[39] Wan L, Gao Z, Moan T. Coastal Engineering, Experimental and Numerical Study of the Hydrodynamic Responses of a Combined Wind and Wave Energy Converter Concept in Survival Modes. Coastal Engineering 2015:104:151–169.

[40] Wan L, Gao Z, Moan T, Lugni C. Comparative experimental study of the survivability of a combined wind and wave energy converter in two testing facilities. Ocean Engineering 2016:111:82–94.

[41] Courbois A. Etude expérimentale du comportement dynamique d'une éolienne offshore flottante soumise à l'action conjuguée de la houle et du vent. Ph.D. thesis, Ecole Centrale de Nantes 2013 (in french).

[42] Scheiman J, Brooks JD. 1981. Comparison of experimental and theoretical turbulence reduction from screens, honeycomb, and honeycomb-screen combinations. Journal of Aircraft 1981:18(8):638–643.

[43] Jonkman J, Butterfield S, Musial W, Scott G. Definition of a 5-MW Reference Wind Turbine for Offshore System Development. Technical Report, NREL/TP-500-38060, National Renewable Energy Laboratory, Boulder, 2009.

[44] MARINTEK. Simo User's Manual 2011. Trondheim, Norway.

[45] MARINTEK. Riflex User's Manual 2013. Trondheim, Norway.

[46] Luan C, Michailides C, Gao Z, Moan T. Modeling and analysis of a 5 MW semi-submersible wind turbine combined with three flap-type Wave Energy Converters. Proc of the 33rd International Conference on Ocean, Offshore and Arctic Engineering, no.OMAE2014-24215, pp. V09BT09A028, doi:10.1115/OMAE2014-24215.

[47] WAMIT. User Manual – program version 6.4 2009 WAMIT Inc. Available at: http:// www.wamit.com. [Accessed in October 2015].

[48] Sojo M, Auer G. D1.12 – Final Summary Report. EU FP7 MARINA Platform Project 2014. Acciona Energia.

Figure Captions

Figure 1. Artistic view of the SFC at sea

Figure 2. Plan view of the experimental set-up of functionality tests of SFC at ECN

Figure 3. Physical model of the SFC in ECN's ocean basin

Figure 4. Plan view (Fig. 4a) and side view (Fig. 4b) of the SFC in full scale

Figure 5. Physical model set-up of the WEC_2 of the SFC

Figure 6. Physical model set-up of the wind turbine of the SFC and wind generation system

Figure 7. Tension of mooring lines ML_2 and ML_3 for different quasi-static forced offset in X direction

Figure 8. Experimental and numerical RAOs of surge (Fig. 8a), heave (Fig. 8b) and pitch (Fig. 8c) of semisubmersible platform and of rotation, θ, of WEC_2 (Fig. 8d) for regular wave without and with wind loading $U_{W,R}$

Figure 9. Experimental and numerical RAOs of tension of the mooring line ML_2

Figure 10. Experimental and numerical RAOs of the nacelle acceleration in the X direction (Fig. 10a) and the bending moment, MX, in the tower's base (Fig. 10b)

Figure 11. Experimental and numerical RAO of FZ_1 of WEC_2 (Fig. 11a), produced power of WEC_2 (Fig. 11b), PTO's torque of WEC_2 (Fig. 11c) and PTO's torque of WEC_3 (Fig. 11d)

Figure 12. Time series of wave elevation (Fig. 12a) for EC2, spectra of wave elevation (Fig 12b) for the EC1, EC2 and EC3, wind speed (Fig. 12c) for EC2 and shear force response on the tower top (Fig. 12d) for EC2

Figure 13. Maximum and std values of surge, heave and pitch of platform for ECi, i=1~6

Figure 14. Maximum and std values of X acceleration of nacelle (Fig. 14a), MX bending moment of the tower's base (Fig. 14b) and tension of the ML_2 (Fig. 14c) for ECi, i=1~6

Figure 15. Maximum and std values of FZ_1 (Fig. 15a), MX_1 WEC_2 (Fig. 15b), torque (Fig. 15c) of WEC_2 and torque (Fig. 15d) of WEC_3 for ECi, i=1~6

Figure 16. Comparison of experimental and numerical response spectra for EC2 and EC5

Figure 1. Artistic view of the SFC at sea

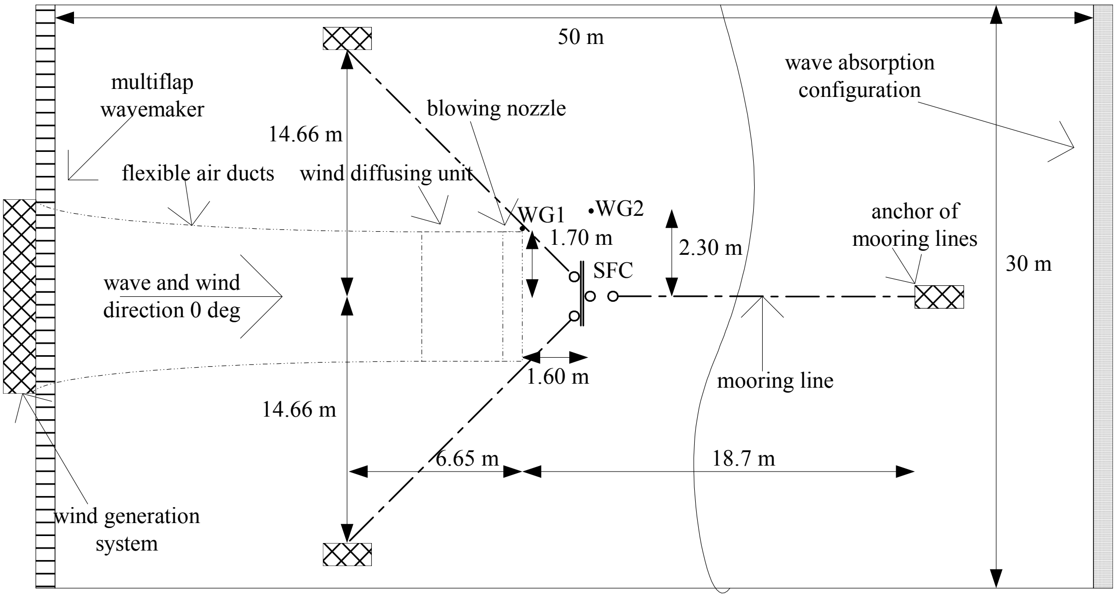

Figure 2. Plan view of the experimental set-up of functionality tests of SFC at ECN

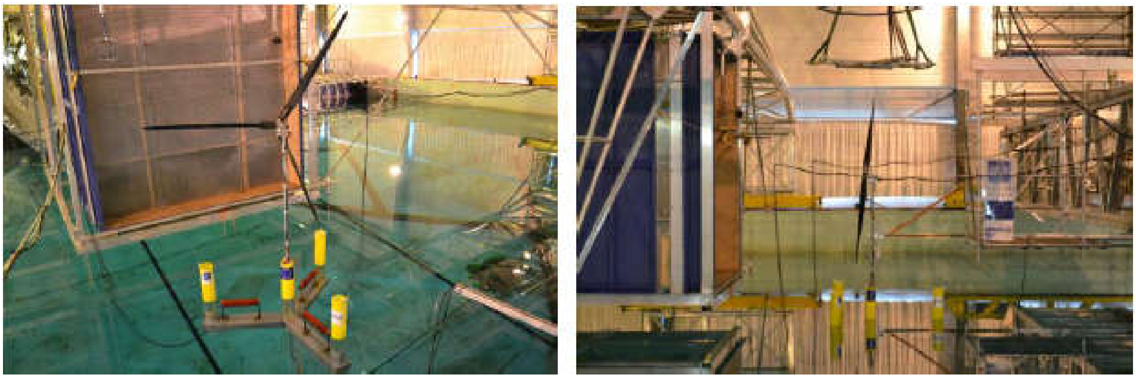

(a) (b)

Figure 3. Physical model of the SFC in ECN’s ocean basin

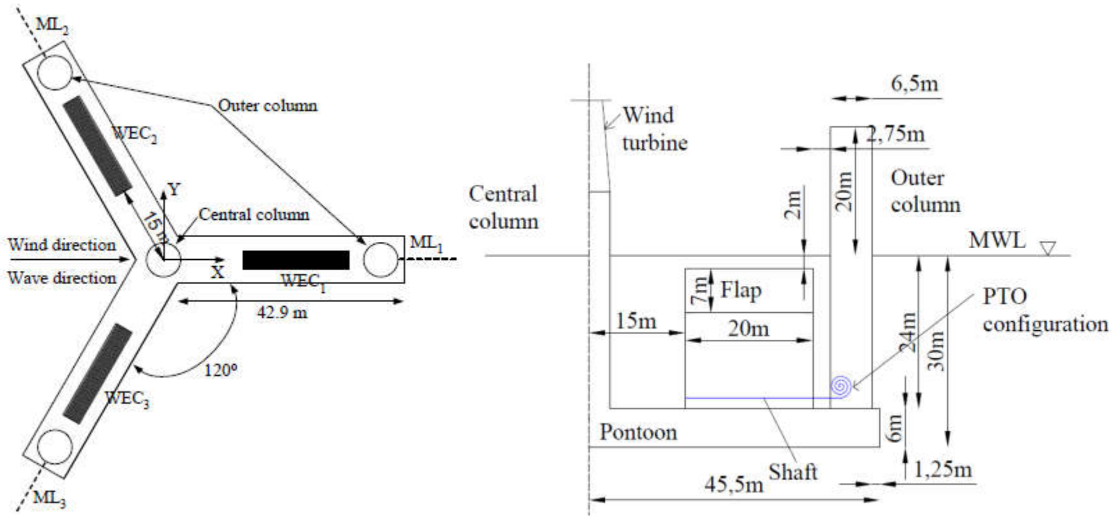

(a) (b)

Figure 4. Plan view (Fig. 4a) and side view (Fig. 4b) of the SFC in full scale

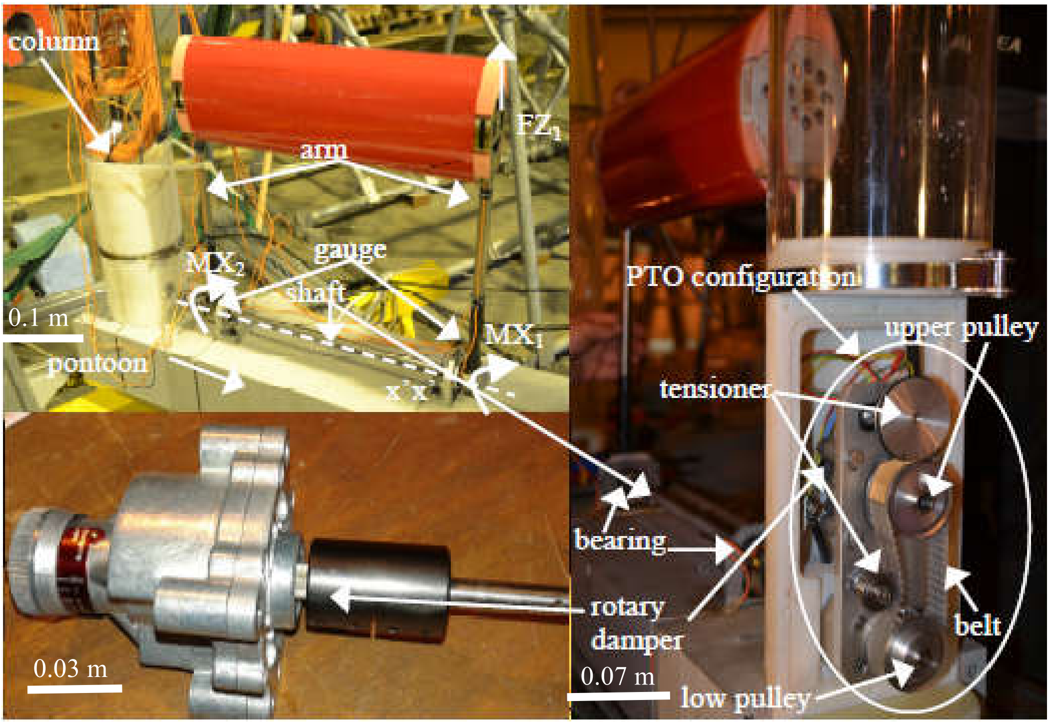

Figure 5. Physical model set-up of the WEC_2 of the SFC

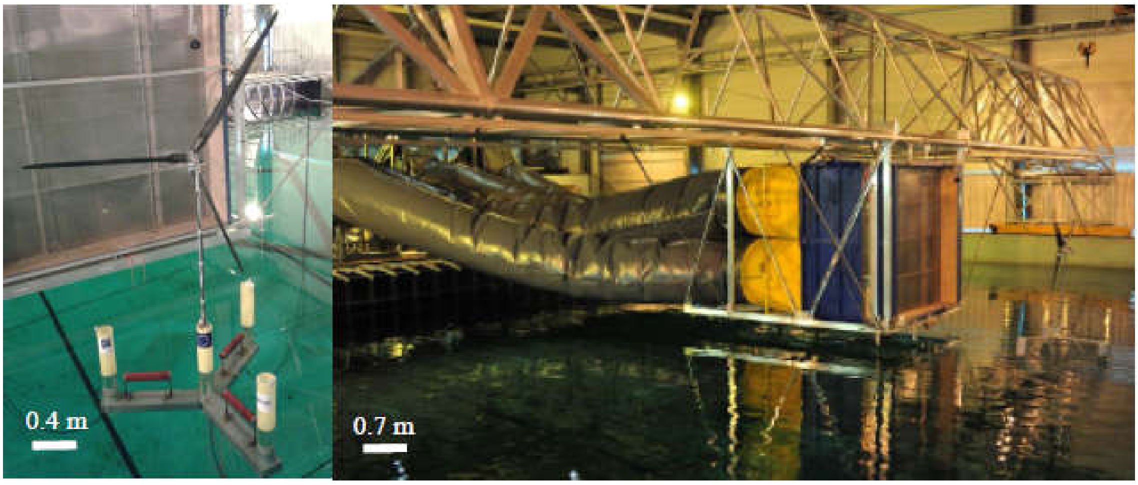

Figure 6. Physical model set-up of the wind turbine of the SFC and wind generation system

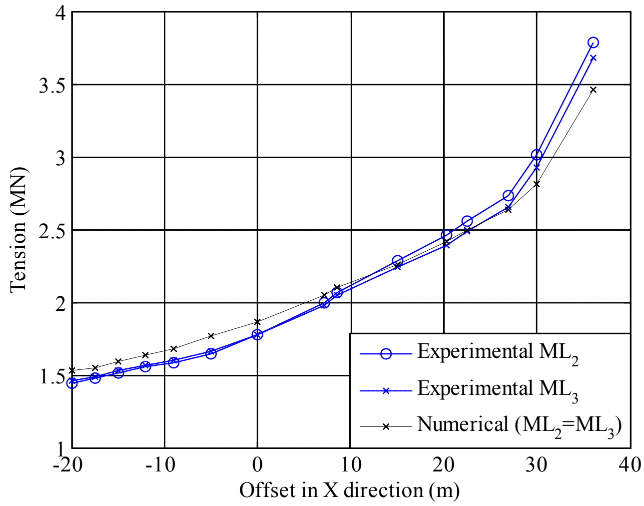

Figure 7. Tension of mooring lines ML_2 and ML_3 for different quasi-static forced offset in X direction

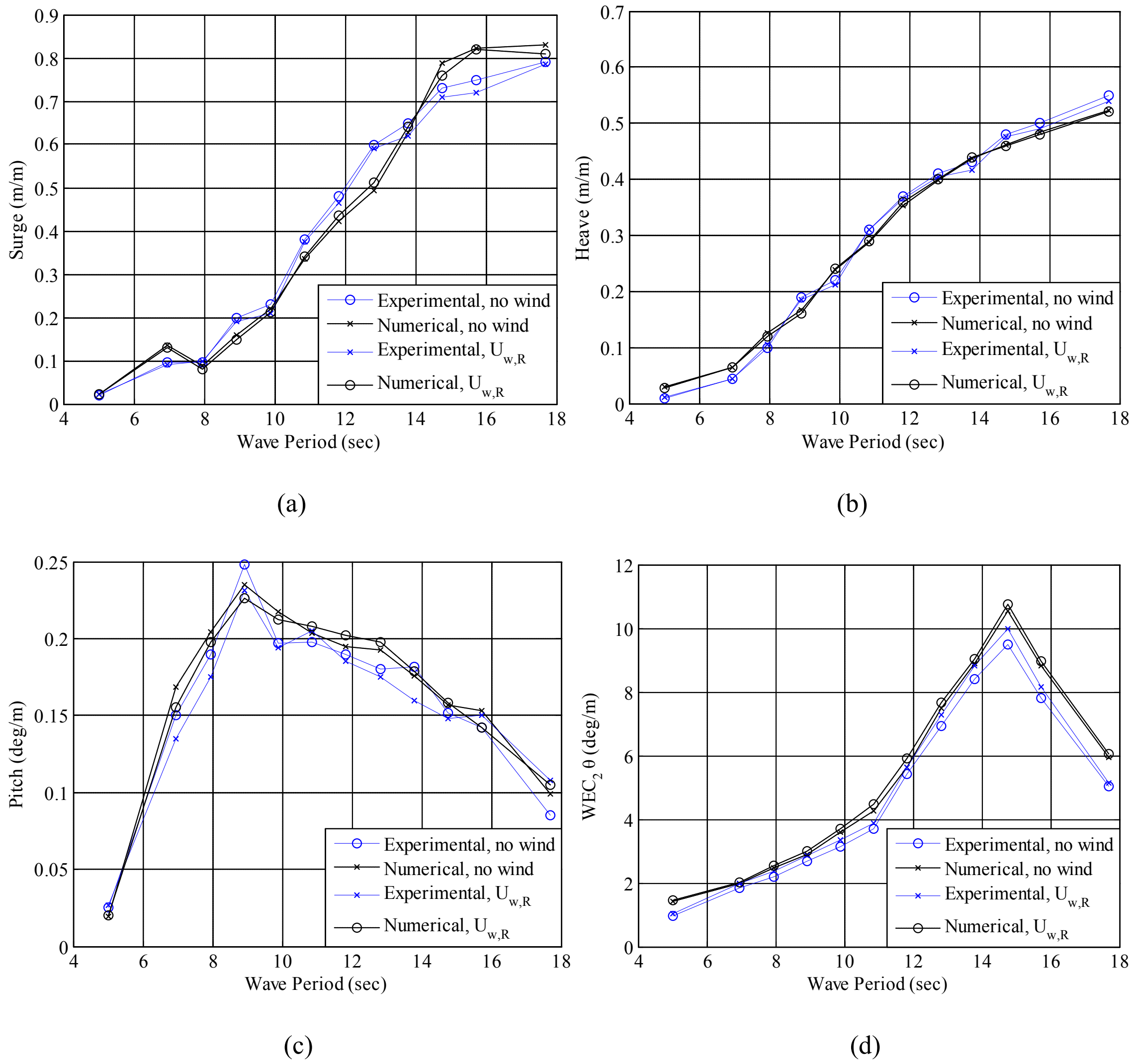

Figure 8. Experimental and numerical RAOs of surge (Fig. 8a), heave (Fig. 8b) and pitch (Fig. 8c) of semisubmersible platform and of rotation, θ, of WEC_2 (Fig. 8d) for regular wave without and with wind loading $U_{W,R}$

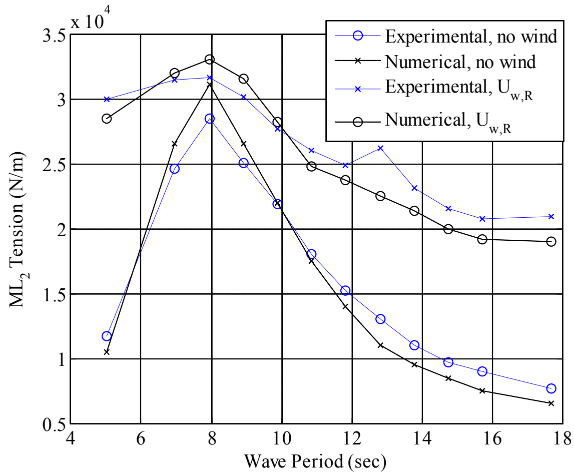

Figure 9. Experimental and numerical RAOs of tension of the mooring line ML_2

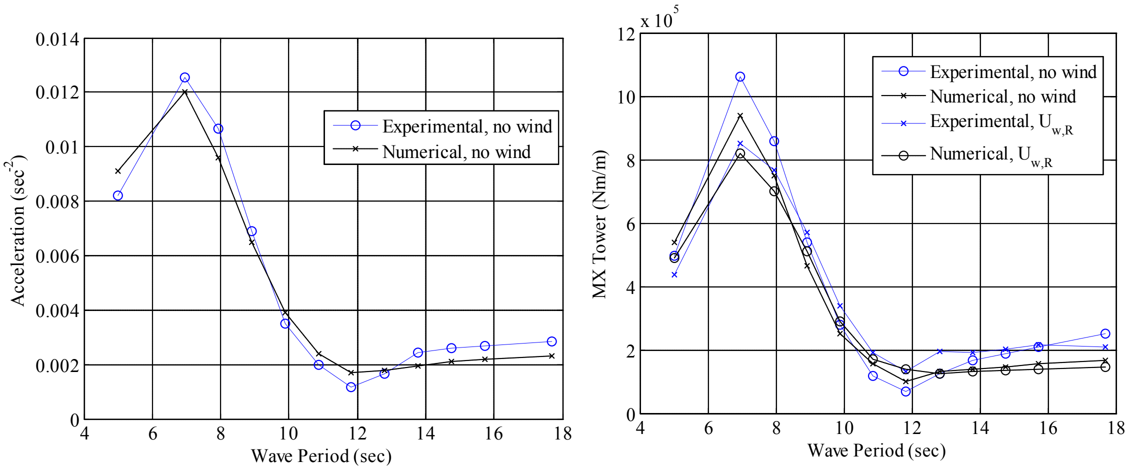

(a) (b)

Figure 10. Experimental and numerical RAOs of the nacelle acceleration in the X direction (Fig. 10a) and the bending moment, MX, in the tower's base (Fig. 10b)

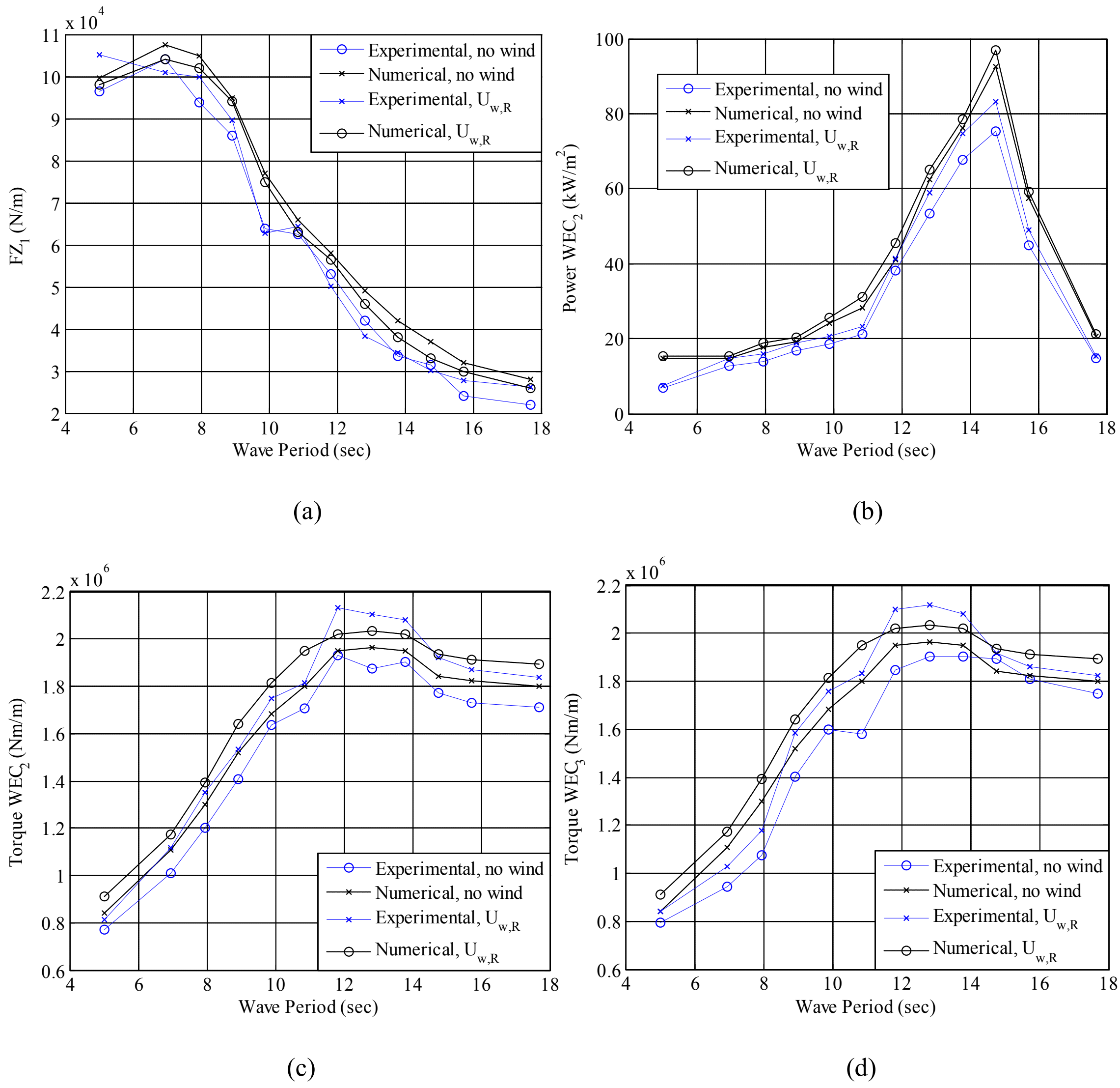

Figure 11. Experimental and numerical RAO of FZ_1 of WEC_2 (Fig. 11a), produced power of WEC_2 (Fig. 11b), PTO's torque of WEC_2 (Fig. 11c) and PTO's torque of WEC_3 (Fig. 11d)

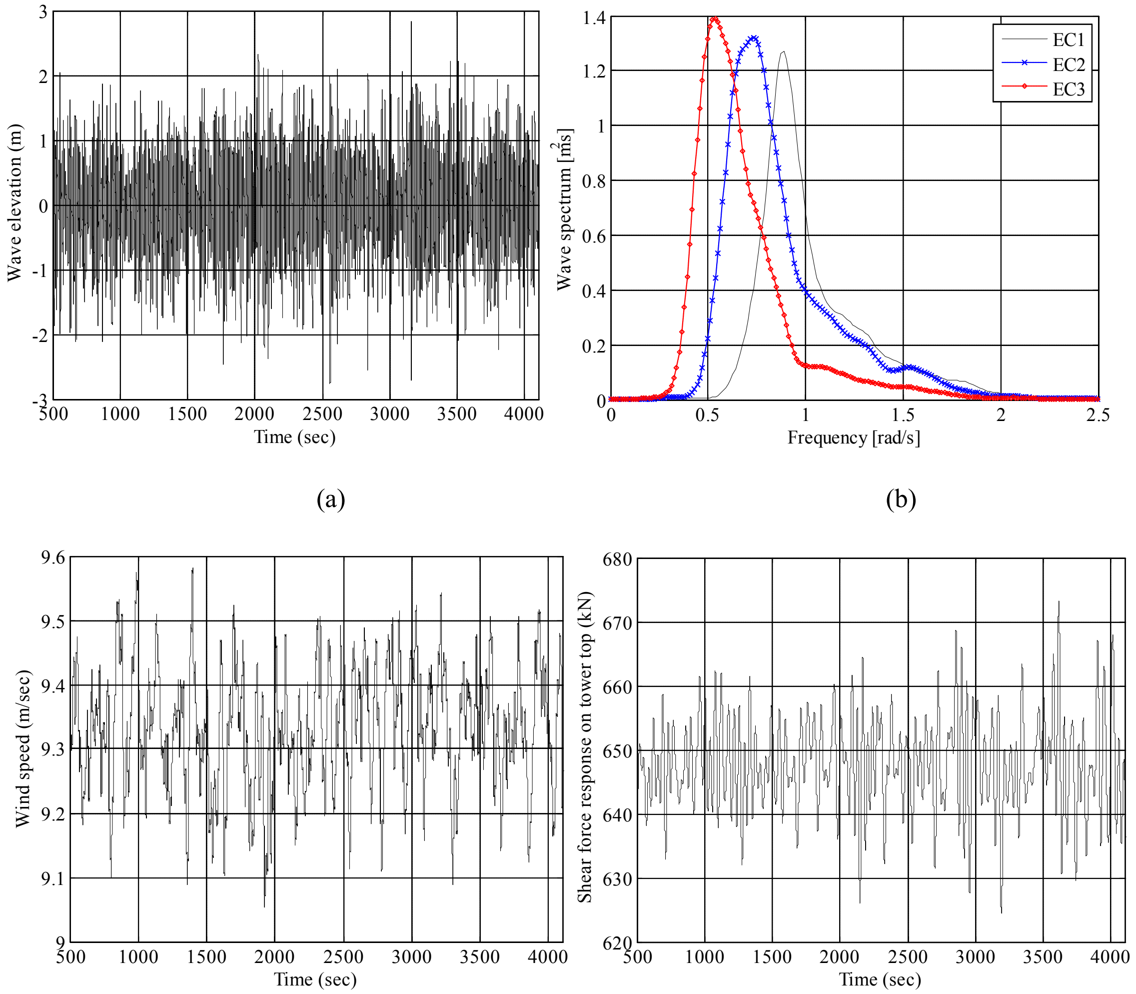

(a) (b)

(c) (d)

Figure 12. Time series of wave elevation (Fig. 12a) for EC2, spectra of wave elevation (Fig 12b) for the EC1, EC2 and EC3, wind speed (Fig. 12c) for EC2 and shear force response on the tower top (Fig. 12d) for EC2

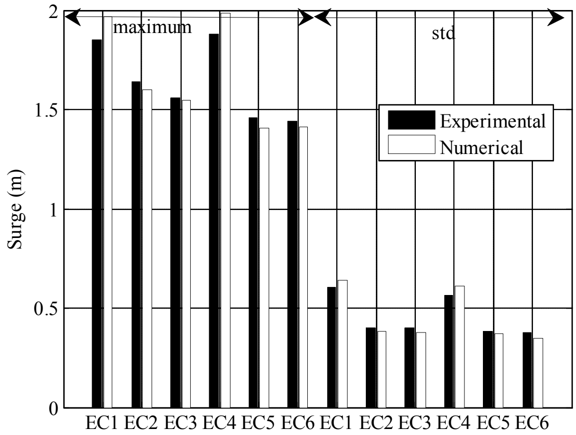

(a)

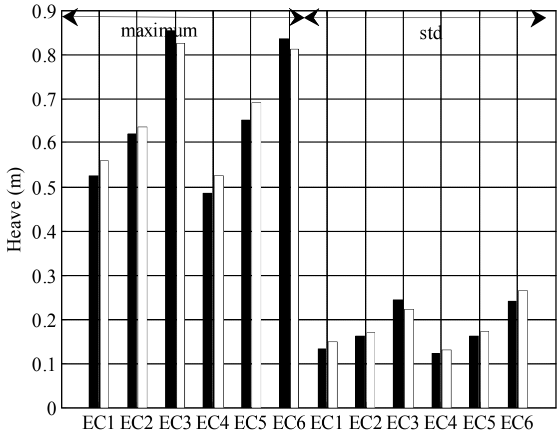

(b)

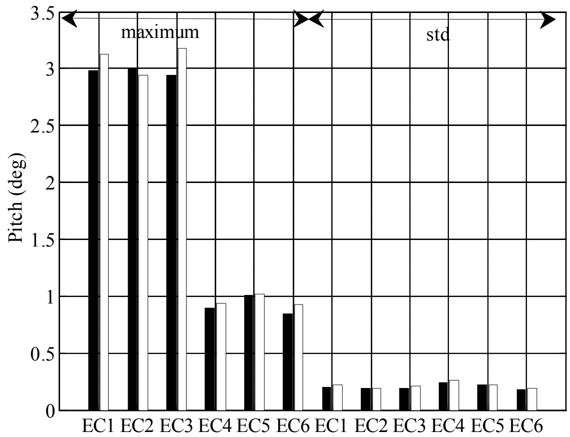

(c)

Figure 13. Maximum and std values of surge, heave and pitch of platform for ECi, i=1~6

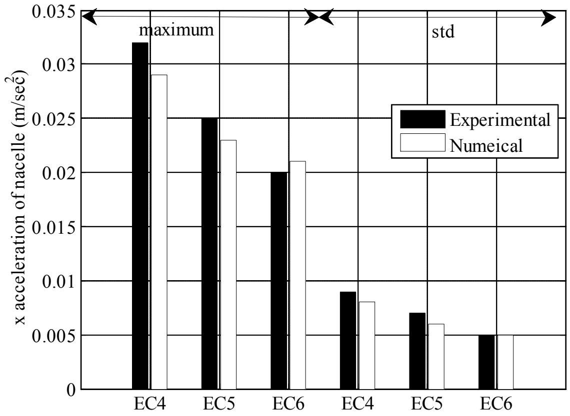

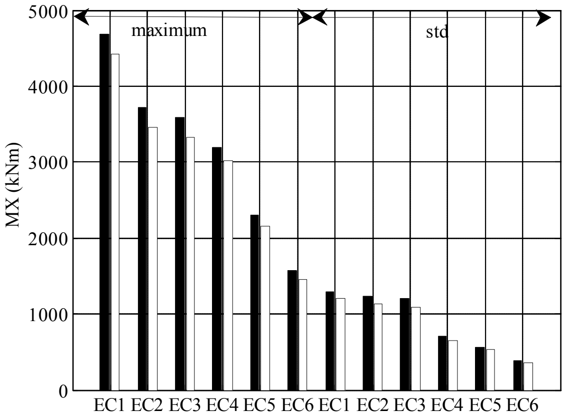

(a) (b)

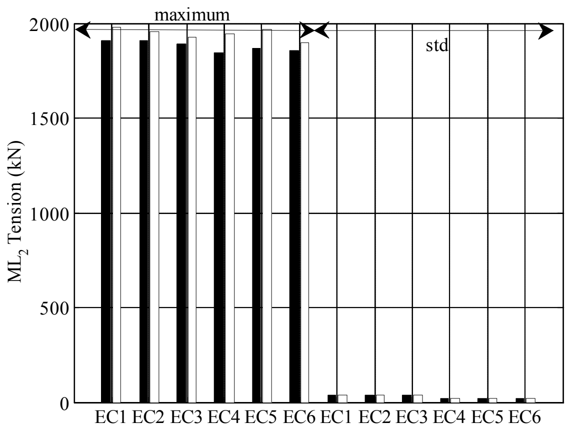

(c)

Figure 14. Maximum and std values of X acceleration of nacelle (Fig. 14a), MX bending moment of the tower's base (Fig. 14b) and tension of the ML_2 (Fig. 14c) for ECi, i=1~6

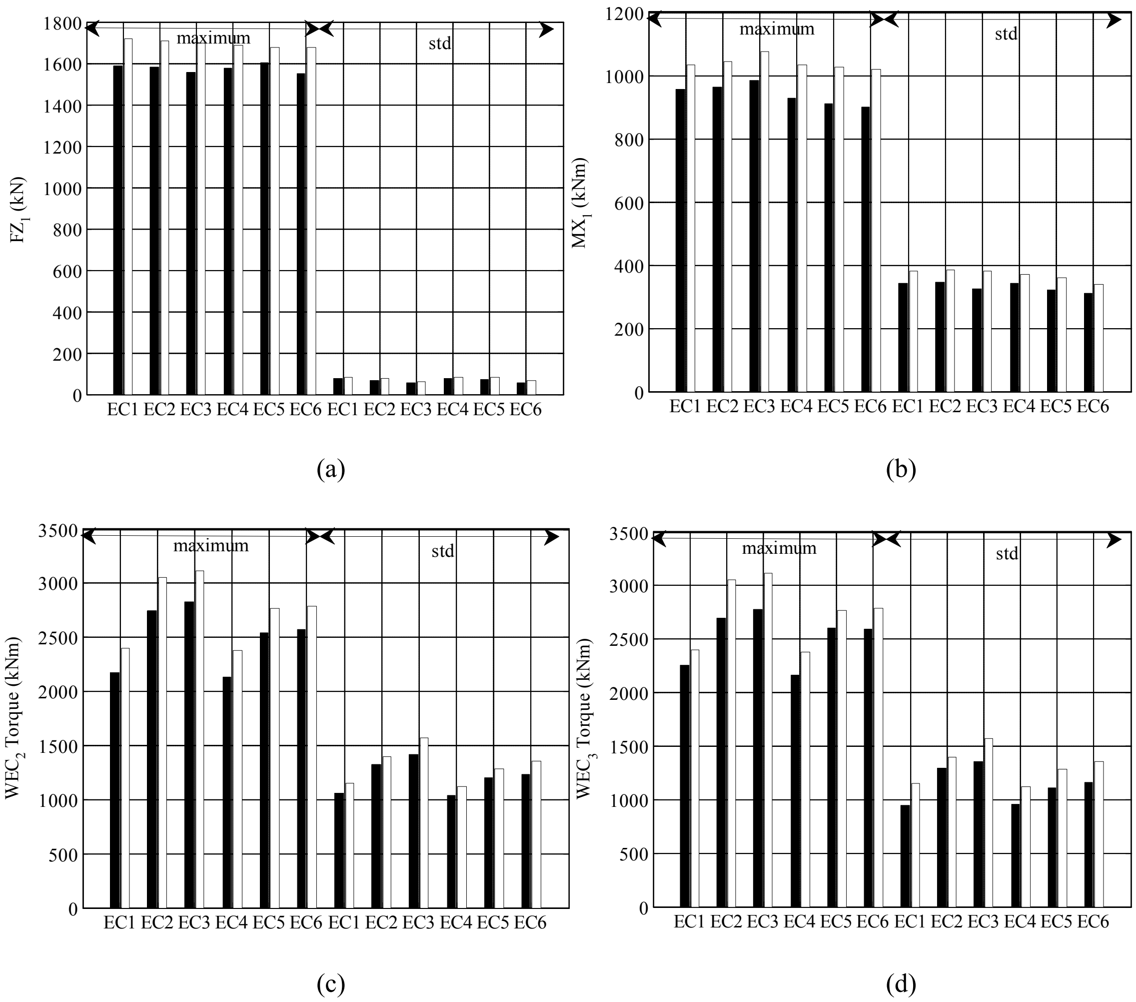

Figure 15. Maximum and std values of FZ_1 (Fig. 15a), MX_1 of WEC_2, (Fig. 15b), torque (Fig. 15c) of WEC_2 and torque (Fig. 15d) of WEC_3 for ECi, i=1~6

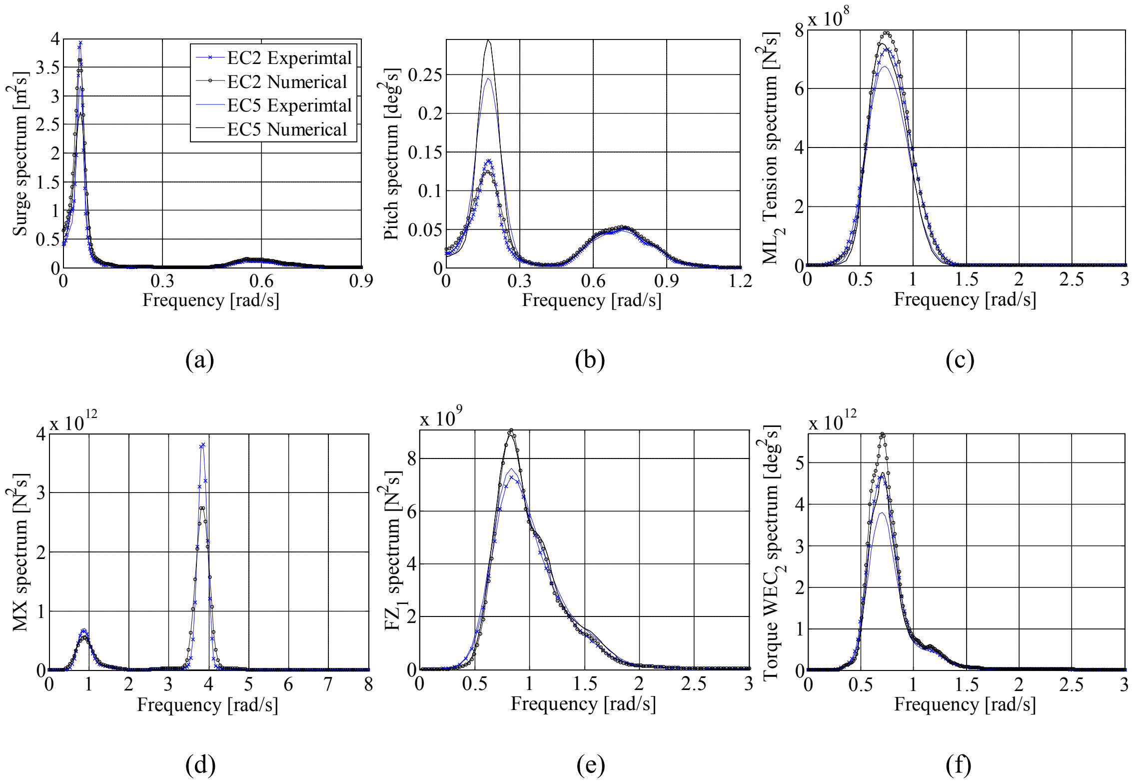

Figure 16. Comparison of experimental and numerical response spectra for EC2 and EC5

Table 1. Scaling of different variables using the Froude laws of similitude for the physical modelling of the properties of the semisubmersible platform and rotating flap-type WECs

Variables	Scale factor	
Linear dimensions (length, height, width, wave height etc)	λ	50
Mass, Force	λ^3	125,000
Time, Velocity	$\lambda^{0.5}$	7.07
Moment	λ^4	6,250,000
Angular motion, Acceleration	1	1
Produced power by WECs	$\lambda^{3.5}$	883,883.5

Table 2. Dimensions and characteristics of the main components of the SFC in full scale values

Properties	Full scale value	Properties	Full scale value
Diameter of the center and outer columns [m]	6.5	Length of the flap[m]	20
Height of the pontoon [m]	6	Height of the flap [m]	7
Width of the pontoon [m]	9	Elliptical axis of flap [m]	3.5
Distance from the center line of the center column to the edge of the pontoon [m]	45.5	Mass of each flap [kg]	100,000
Draft [m]	30	Displacement of each flap [kg]	395,000
COG of the whole SFC (x,y,z) [m]	(0,0,-0.367)	WEC Ix'x' local coordinate system (kg*m^2)	656,250
Ixx (kg*m^2)	11,445,542,000	WEC Iy'y' (kg*m^2)	4,496,875
Iyy (kg*m^2)	11,445,542,000	WEC Iz'z' (kg*m^2)	4,168,750
Izz (kg*m^2)	9,772,627,000	Wind turbine	NREL 5MW

Table 3. Structural properties of the blades of the wind turbine (model scale)

Variables	SFC	NREL target
Length [m]	1.223	1.23
Mass [kg]	0.135	0.145
First Flapwise flexible mode [Hz]	7.3	4.74

Table 4. Structural properties of the nacelle and hub of the wind turbine (model scale)

Variables	SFC	NREL target
Nacelle mass [kg]	1.95	1.97
Shaft tilt [º]	5	5
Hub mass [kg]	0.635	0.47
Vertical distance of hub to the MWL [m]	1.8	1.8
Hub diameter [m]	0.06	0.06
Horizontal distance of hub to the tower [m]	0.0996	0.100

Table 5. Examined wave periods for regular wave tests (wave height of 2 m)

T_1 (sec)	T_2 (sec)	T_3 (sec)	T_4 (sec)	T_5 (sec)	T_6 (sec)
5.013	6.965	7.934	8.910	9.885	10.861
T_7 (sec)	T_8 (sec)	T_9 (sec)	T_{10} (sec)	T_{11} (sec)	T_{12} (sec)
11.830	12.806	13.782	14.757	15.726	17.678

Table 6. Examined operational environmental conditions ECi, i=1~6

ECi, i=1~6	H_s (m)	T_p (sec)	U_w (m/sec)	TI
EC1	3.0	7.0	9.35	0.009
EC2	3.0	9.0	9.35	0.009
EC3	3.0	12.0	9.35	0.009
EC4	3.0	7.0	-	-
EC5	3.0	9.0	-	-
EC6	3.0	12.0	-	-

Table 7. Natural periods of surge, heave and pitch motion of the platform and of rotation of WEC_2 obtained from numerical and experimental decay tests (full scale values)

Degree of freedom	T_{exp} (sec)	T_{num} (sec)	ξ_{exp} (%)
Surge	113.066	113.561	4.0
Heave	26.233	26.517	2.8
Pitch	34.548	34.790	4.9
WEC_2 rotation	14.483	14.920	7.2

Table 8. Statistical quantities of produced power of WEC_2

ECi	Mean (kW)		Std (kW)		Maximum (kW)	
	Experimental	Numerical	Experimental	Numerical	Experimental	Numerical
EC1	47.3	55.7	72.1	85.0	890.2	1029.1
EC2	57.7	63.9	82.9	92.1	924.8	1066.4
EC3	70.2	77.6	101.6	114.1	996.2	1119.3
EC4	43.3	50.7	66.1	77.4	815.5	904.9
EC5	50.9	56.3	73.17	81.0	836.5	953.9
EC6	61.2	68.1	88.6	100.3	868.8	983.1